

Single-ion nonlinear mechanical oscillator

N. Akerman, S. Kotler, Y. Glickman, Y. Dallal, A. Keselman, and R. Ozeri

Physics of Complex Systems, The Weizmann Institute of Science, Rehovot 76100, Israel

(Received 8 March 2010; revised manuscript received 13 June 2010; published 16 December 2010)

We study the steady-state motion of a single trapped ion oscillator driven to the nonlinear regime. Damping is achieved via Doppler laser cooling. The ion motion is found to be well described by the Duffing oscillator model with an additional nonlinear damping term. We demonstrate here the unique ability of tuning both the linear as well as the nonlinear damping coefficients by controlling the laser-cooling parameters. Our observations pave the way for the investigation of nonlinear dynamics on the quantum-to-classical interface as well as mechanical noise squeezing in laser-cooling dynamics.

DOI: [10.1103/PhysRevA.82.061402](https://doi.org/10.1103/PhysRevA.82.061402)

PACS number(s): 37.10.Vz, 05.45.-a, 37.10.Ty

Nonlinear dynamics prevails in many dynamical systems in nature; it introduces a rich behavior that includes criticality, bifurcations, and chaos. Nonlinear dynamics on the microscopic scale is especially interesting because it can shed light on the quantum-to-classical transition [1] as well as provide a means to amplify or suppress thermal and quantum noise [2].

All mechanical oscillators exhibit nonlinearity when driven far away from equilibrium. The simplest of such nonlinear oscillators is the Duffing oscillator, which includes a cubic term in the restoring force [3]. Duffing nonlinear dynamics has been studied with electrons in a Penning trap [4] and recently with nano-electromechanical beam resonators. The basins of attraction of a nanobeam oscillator were mapped [5]. Noise squeezing and stochastic resonances were observed close to the Duffing instability [6,7]. Noise squeezing was predicted to enable mass and force detection with precision below the standard thermal limit [8–10] and possibly below the standard quantum limit when operating close to the oscillator ground state [11].

The mechanical motion of trapped ions is highly controllable and can be efficiently laser-cooled to the quantum ground state [12]. High-fidelity production of Fock, squeezed, and Schrödinger-cat states was demonstrated with a single trapped ion [13,14]. At the temperature range obtained with laser-cooling techniques, quadruple radiofrequency (rf) Paul traps are excellently approximated as harmonic. Nonlinearity in ion motion was observed when several ions were trapped due to their mutual Coulomb repulsion. Here, nonlinearity couples between the ion-crystal normal modes, even at the single quantum level [15,16]. Trap nonlinearities are important in the context of resonance ejection in high-resolution mass spectrometry [17] and were shown to introduce instabilities in the ion motion at certain trapping parameters [18]. Recently, amplification saturation of a single-ion “phonon laser,” resulting from optical forces that are nonlinear in the ion velocity, was demonstrated [19].

Here, we study the nonlinear mechanical response of a single laser-cooled $^{88}\text{Sr}^+$ ion in a linear rf Paul trap. The nonlinearity originates from the higher than quadrupolar order terms in the trapping potential. We find that the ion’s steady-state response is well described by the Duffing model with an additional nonlinear damping term [20]. Unlike other realizations of nonlinear mechanical oscillators, both the linear and the nonlinear damping components can be precisely controlled.

Our trap has a canonical linear configuration featuring four rods and two end caps, as shown in Fig. 1. The distance from the ion to the end caps and rod electrodes is 0.65 and 0.27 mm, respectively. Here we examined only the motion along the axial direction of the trap. In this direction, trapping is dominated by the static electric potential due to positive constant voltage on the trap end caps. This potential is well approximated to be harmonic with $\omega_0/2\pi = 438$ kHz. However, since the trap end caps do not satisfy the pure electric quadrupole boundary condition, a small octupolar contribution to the electric field results in a positive cubic term in the restoring force and an energy-level difference of $\hbar\omega_0 + \hbar\Delta_{nl}n$, where n is the harmonic-oscillator quantum number and $\Delta_{nl}/2\pi = 0.8$ mHz is the nonlinear dispersion. This nonlinearity becomes more important with increasing oscillation amplitude. The ion is driven to the nonlinear regime by adding a small oscillating voltage to one of the trap end caps.

The ion is Doppler-cooled by scattering photons from a single laser beam, slightly red-detuned from the $S_{1/2} \rightarrow P_{1/2}$ transition at 422 nm. To prevent population accumulation at the $D_{3/2}$ metastable level, we repump the ion on the $D_{3/2} \rightarrow P_{1/2}$ transition at 1092 nm.

We measure the steady-state oscillation amplitude of the ion as we slowly scan the drive frequency detuning, $\sigma = \omega - \omega_0$, across the harmonic resonance, ω_0 . The scan is from lower to higher frequencies (a positive sweep) or vice versa (a negative sweep). Photons scattered during the cooling process are collected by an imaging system (numerical aperture of 0.31) and are either directed toward an electron-multiplying charge-coupled-device (EMCCD) camera or a photomultiplier tube (PMT).

We measure the amplitude of motion by taking time-averaged images of the ion. Six such images for various drive frequencies are presented in Fig. 2(a). The image is then integrated along the direction perpendicular to the motion to produce a single curve. Every column in Fig. 2(b) corresponds to a curve produced in this way for a positive frequency sweep. As shown, the oscillation amplitude increases as the drive frequency approaches ω_0 . It continues to increase past ω_0 until it reaches a given critical drive frequency detuning, σ_m , and then it abruptly collapses to a significantly lower value. We extract the ion oscillation amplitude by fitting the curve to the expected time-averaged position distribution. The blue and red lines in Fig. 3 represent the measured amplitudes for positive and negative sweeps, respectively. Different curves correspond

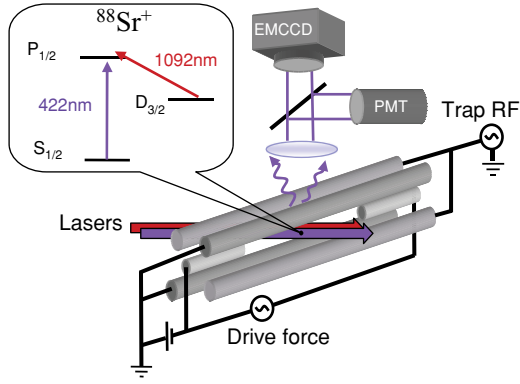


FIG. 1. (Color) Schematic diagram of the experimental setup and the relevant energy levels of the $^{88}\text{Sr}^+$ ion. The positively biased trap end caps produce a static trapping potential in the axial direction with small anharmonicity. The ion oscillator is driven to the nonlinear regime by a small oscillating voltage on one of the trap end caps. Violet and infrared laser beams provide laser cooling and optical pumping. Scattered violet photons are collected by an imaging system and directed either to an EMCCD camera or to a PMT.

to different drive amplitudes. The asymmetry and hysteresis as well as the abrupt amplitude changes at specific critical drive frequencies clearly deviate from the driven harmonic-oscillator response. As expected from positive nonlinearity, the oscillator self-frequency is “pulled” to higher values at higher oscillation amplitudes.

In order to measure the phase difference between the ion oscillator and the driving force, we time-stamp each photon measured by the PMT within a single drive period to allocate it

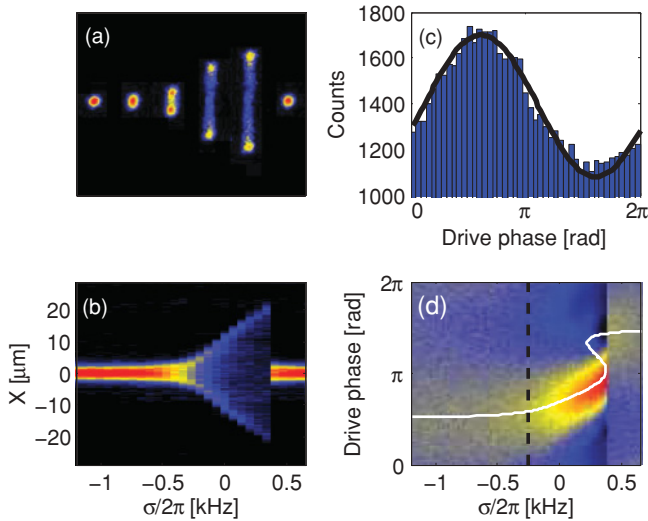


FIG. 2. (Color) Driven ion-oscillator amplitude and phase. (a) Time-averaged ion images taken at various drive frequencies. (b) Columns are time-averaged images, integrated along the direction perpendicular to the ion motion, during a positive frequency scan. (c) A histogram of the number of photons detected at different driving force phases. (d) Columns are photon phase histograms taken during a single, 3-h-long positive frequency scan. The solid line denotes the theoretical phase given by Eq. (3) shifted by $\pi/2$ due to a constant phase difference between the ion’s position and its photon-scattering rate.

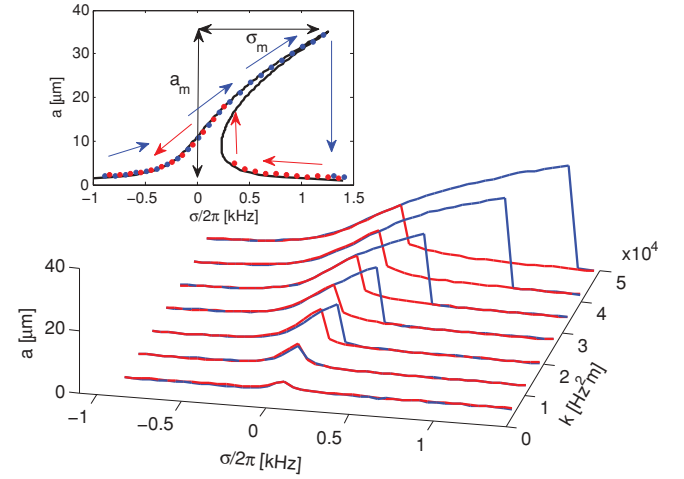


FIG. 3. (Color) Measured oscillator amplitude vs drive frequency for various driving force amplitudes and both positive (blue) and negative (red) scans. The inset shows the Duffing model calculation (black solid line) and our measured amplitudes (blue circles, positive scan; red circles, negative scan).

with a corresponding drive phase. The instantaneous photon-scattering rate from the laser-cooling beam is determined by the ion’s instantaneous velocity through its associated Doppler shift [21]. A histogram of the measured photon phases is shown in Fig. 2(c). A clear sinusoidal oscillation of the photon-scattering rate indicates the ion-oscillator phase. The columns in Fig. 2(d) are photon phase histograms for a positive drive frequency sweep. As shown, at the critical drive detuning frequency, σ_m , a sudden change in oscillation amplitude is accompanied by a phase jump of 1.2 radians in the oscillator motion.

Our observations are well accounted for by the Duffing oscillator model. The Duffing equation of motion is

$$\ddot{x} + 2\mu\dot{x} + \omega_0^2x + \alpha x^3 = k \cos(\omega t). \quad (1)$$

Here x is the displacement of the ion from its equilibrium position, α is the anharmonic coefficient, μ is the linear damping coefficient resulting from the recoil associated with the absorption of photons from the laser-cooling beam, and k is the drive’s amplitude. The recoil noise, inherent to the spontaneous photon-emission process, is neglected here because the resulting thermal amplitude is at least two orders of magnitude smaller than the typical oscillation amplitude in the nonlinear regime. An approximate solution to Eq. (1) can be obtained by the multiple scale method [3]. Here the solution has the form $x(t) = a(t) \cos(\omega t - \phi)$, where $a(t)$ denotes a slowly varying oscillation amplitude and ϕ represents the oscillator phase. The steady-state solution for a is solved by

$$\sigma = \frac{3\alpha}{8\omega_0} a^2 \pm \sqrt{\frac{k^2}{4\omega_0^2 a^2} - \mu^2}. \quad (2)$$

The steady-state solution for a , at a fixed k , versus drive frequency is denoted by the black line in the inset of Fig. 3. Above a critical amplitude a_c , a separates into three solutions. One solution with a small amplitude and one with a large amplitude are stable, whereas the third, intermediate-amplitude solution, is unstable and is positioned

on the state-space separatrix. This bistability persists until the high-amplitude solution reaches a maximal value a_m . At that point, the drive force is overwhelmed by damping and the oscillator is forced into a single stable solution. Positive and negative frequency scans carry the oscillator into the bistability region along different stable attractors, leading to the observed hysteresis, as illustrated by the arrows in the inset. To compare with our data, we independently measured all the parameters in Eq. (1). The driving force amplitude k is measured by observing ion displacement versus end-cap voltage, and ω_0 is measured via ion response in the linear regime. A value of $\alpha/4\pi^2 = 1.24 \pm 0.03 \times 10^{18} \text{ Hz}^2/\text{m}^2$ was measured using the observed dependence of a_m on the instability detuning σ_m , $a_m = \sqrt{8\omega_0\sigma_m/3\alpha}$. A value of $\mu/2\pi = 39.2 \pm 0.3 \text{ Hz}$, which resulted in a quality factor $Q = 5590$, was evaluated using the variation of a_m with the drive amplitude, $a_m = k/(2\mu\omega_0)$. The blue and red circles in the inset represent the measured amplitudes for positive and negative scans, respectively, showing good agreement with the theoretical curve.

The Duffing oscillator steady-state phase is given by

$$\tan(\phi) = \frac{8\mu\omega_0}{3\alpha a^2 - \omega_0\sigma}. \quad (3)$$

The white solid line in Fig. 2(d) represents the theoretical phase curve versus the drive frequency for our experimental parameters, showing good agreement with our data.

Linear damping is a very good approximation for most mechanical oscillators, since typically dissipation originates from coupling of the oscillator to an Ohmic bath. Recently, the contribution of nonlinear damping to the motion of a nanobeam resonator was studied [23]. In our experiment, damping results from the change in radiation pressure versus ion velocity. When the laser frequency is tuned below the cooling transition, the leading contribution is indeed linear in the ion velocity. However, as the oscillation amplitude increases or the laser-cooling detuning is reduced, the effect of the damping force terms that are nonlinear in the ion velocity increases [21].

To account for nonlinear damping, Eq. (1) was modified to include a term that is cubic in the oscillator velocity,

$$\ddot{x} + 2\mu\dot{x} + \gamma\dot{x}^3 + \alpha x^3 = k \cos(\omega t). \quad (4)$$

Here γ is the cubic damping coefficient. The steady-state amplitude is now a solution of [22,23]

$$\frac{9}{16}(\alpha^2 + \gamma^2\omega_0^6)a^6 + 3\omega_0(\mu\gamma\omega_0^3 - \sigma\alpha)a^4 + 4\omega_0^2(\sigma^2 + \mu^2)a^2 - k^2 = 0. \quad (5)$$

When $\gamma > 0$, nonlinear damping effectively increases dissipation for larger oscillation amplitudes. Unlike the case of linear damping, a_m does not increase linearly with k but is instead limited by the growing dissipation. We found μ and γ by a maximum likelihood fit of the measured a_m versus k curve to the solution of Eq. (5). It is instructive to look at the responsivity, $\chi = 2\mu\omega_0 a/k$, in order to distinguish linear from nonlinear damping [22]. Figure 4 plots the measured χ for positive scans and various drive amplitudes, k , for two different laser-cooling detuning values, δ . In Fig. 4(a), $\delta/2\pi = -420 \text{ MHz}$, $\gamma = 0$, and the maximal responsivity is

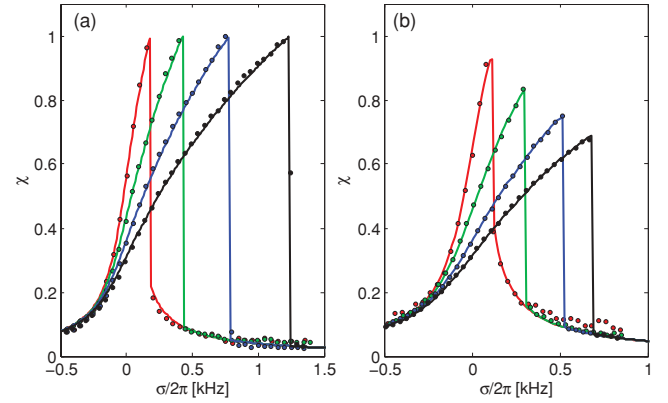


FIG. 4. (Color) Calculated and measured responsivity, $\chi = 2\mu\omega_0 a/k$, for positive drive scans. Different curves correspond to different drive amplitudes. Due to small drifts in ω_0 ($< 100 \text{ Hz}$), each curve was shifted separately on the frequency axis to fit the theoretical curve. (a) Linear damping, the laser-cooling detuning $\delta/2\pi = -420 \text{ MHz}$, and $\gamma = 0$. The maximal responsivity is independent of drive amplitude k . (b) Nonlinear damping, $\delta/2\pi = -160 \text{ MHz}$, and $\omega_0^2\gamma/2\pi = 0.09 \mu\text{m}^{-2} \text{ Hz}$. The maximal responsivity decreases as k increases.

seen to be independent of k . In Fig. 4(b), $\delta/2\pi = -160 \text{ MHz}$, $\omega_0^2\gamma/2\pi = 0.09 \pm 0.002 \mu\text{m}^{-2} \text{ Hz}$, and the maximal responsivity decreases as k increases. The linear dissipation term μ is similar in both cases. The solid lines, which represent the solutions of Eq. (5), are in good agreement with the data.

Next, we repeat the measurement of μ and γ for various laser-cooling detunings at a fixed repump laser frequency and laser intensities. The measured μ and γ versus δ are shown in Figs. 5(a) and 5(b), respectively. To compare these values with the theoretically predicted values, we write the laser-cooling scattering force,

$$F_s(\dot{x}) = \hbar k_c \Gamma \rho_p (\delta_c + k_c \dot{x}, \delta_r + k_r \dot{x}), \quad (6)$$

where $k_{c/r}$ and $\delta_{c/r}$ are the wave vectors and detunings of the cooling and repump lasers, respectively, $\Gamma = 2\pi \times 21 \text{ MHz}$

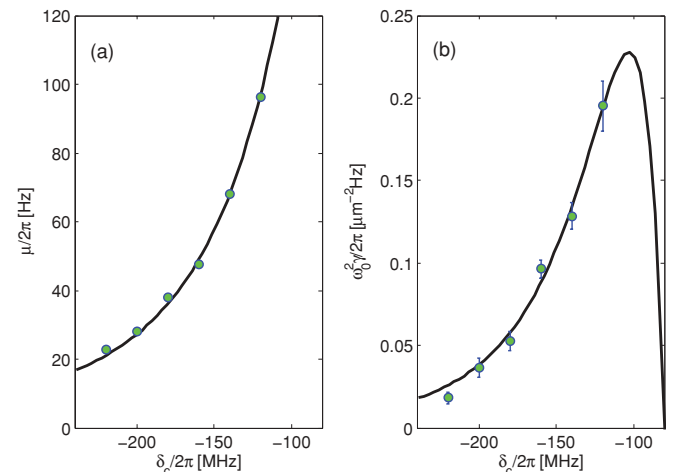


FIG. 5. (Color) (a) Linear and (b) cubic damping coefficients for various cooling-beam detunings. Filled circles denote measured values and solid lines denote calculated values using Eqs. (6) and (7).

is the spectral linewidth of the $P_{1/2}$ level, and ρ_p is the $P_{1/2}$ population. The damping coefficients are, therefore, given by the appropriate derivatives,

$$\mu = \frac{1}{2m} \frac{dF_s}{d\dot{x}}, \quad \gamma = \frac{1}{6m} \frac{d^3F_s}{d\dot{x}^3}. \quad (7)$$

Here m denotes ion mass. We calculate ρ_p by numerically solving the eight coupled Bloch equations, corresponding to the population in all states in the $S_{1/2}$, $P_{1/2}$, and $D_{3/2}$ levels coupled by the cooling and repump lasers. The cubic damping coefficient is highly sensitive to different laser parameters due to the presence of dark resonances. The solid lines in Figs. 5(a) and 5(b), which represent the calculated μ and γ , are in good agreement with our measured values. The two laser intensities and the repump-laser detuning were used as fit parameters, yielding values that agree within 20% of their measured values.

An additional nonlinear damping term, proportional to $x^2\dot{x}$, results from the laser beam's finite size (100 μm full width at half-maximum) and has an effect identical to that of γ regarding the steady-state motion [20,22]. This term was calculated to be small relative to γ [24] and was taken into account in Fig. 5.

In conclusion, we have driven a single-ion oscillator to the nonlinear regime. The ion steady-state motion, exhibiting a bifurcation into two stable attractors and hysteresis, is well described by the Duffing oscillator model with an additional nonlinear damping term. Unlike previously studied nonlinear mechanical oscillators, here both the linear and nonlinear parts of dissipation can be tuned with the laser-cooling parameters.

The high controllability and low temperature of the single-ion nonlinear oscillator opens up several exciting research

avenues. Since trapped atomic ions can be cooled to the quantum ground state, they serve as an excellent platform to study nonlinear behavior in the quantum regime. However, in order to reach this regime, the nonlinearity coefficient α must be enhanced by using a different trap geometry. As shown in [1], a driven Duffing oscillator will show a clear difference between quantum and classical dynamics, with decoherence as the generator of the quantum-classical transition.

The low temperature of the ion oscillator enables operation closer to the instability point than is possible in other mechanical realizations of the Duffing oscillator. Here, weak signal amplification and squeezing will allow us to improve on force measurement sensitivity [25].

Laser cooling of a nonlinear driven ion oscillator has several interesting aspects that can be explored further. Since the Doppler shifts associated with the oscillation amplitudes in the nonlinear regime are significant compared with the cooling transition linewidth, the laser-cooling force is largely nonlinear in the oscillator velocity. Furthermore, the thermal state generated by laser cooling results from the balance between the damping force and the inherent heating due to spontaneous photon emission. Close to the Duffing instability, the ion-oscillator response to noise is quadrature-dependent. One noise quadrature is largely enhanced whereas the other quadrature is suppressed [6]. Laser cooling here is likely to produce squeezed states of motion.

This work was partially supported by the ISF Morasha program, the Crown Photonics Center, and the Minerva Foundation.

-
- [1] S. Habib, K. Shizume, and W. H. Zurek, *Phys. Rev. Lett.* **80**, 4361 (1998).
 - [2] K. Wiesenfeld and B. McNamara, *Phys. Rev. A* **33**, 629 (1986).
 - [3] A. H. Nayfeh and D. T. Mook, *Nonlinear Oscillations*, Wiley Classics Library Series (Wiley, New York, 1995).
 - [4] J. Tan and G. Gabrielse, *Phys. Rev. A* **48**, 3105 (1993).
 - [5] I. Kozinsky, H. W. C. Postma, O. Kogan, A. Husain, and M. L. Roukes, *Phys. Rev. Lett.* **99**, 207201 (2007).
 - [6] R. Almog, S. Zaitsev, O. Shtempluck, and E. Buks, *Phys. Rev. Lett.* **98**, 078103 (2007).
 - [7] R. L. Badzey and P. Mohanty, *Nature (London)* **437**, 995 (2005).
 - [8] B. Yurke, D. S. Greywall, A. N. Pargellis, and P. A. Busch, *Phys. Rev. A* **51**, 4211 (1995).
 - [9] E. Buks and B. Yurke, *Phys. Rev. E* **74**, 046619 (2006).
 - [10] J. S. Aldridge and A. N. Cleland, *Phys. Rev. Lett.* **94**, 156403 (2005).
 - [11] E. Babourina-Brooks, A. Doherty, and G. J. Milburn, *New J. Phys.* **10**, 105020 (2008).
 - [12] D. Leibfried, R. Blatt, C. Monroe, and D. J. Wineland, *Rev. Mod. Phys.* **75**, 281 (2003).
 - [13] D. M. Meekhof, C. Monroe, B. E. King, W. M. Itano, and D. J. Wineland, *Phys. Rev. Lett.* **76**, 1796 (1996).
 - [14] C. Monroe, D. M. Meekhof, B. E. King, and D. J. Wineland, *Science* **272**, 1131 (1996).
 - [15] C. Marquet, F. Schmidt-Kaler, and D. F. V. James, *Appl. Phys. B* **76**, 199 (2003).
 - [16] C. F. Roos *et al.*, *Phys. Rev. A* **77**, 040302(R) (2008).
 - [17] A. A. Makarov, *Anal. Chem.* **68**, 4257 (1996).
 - [18] A. Drakoudis, M. Sollner, and G. Werth, *Int. J. Mass Spectrom.* **252**, 61 (2006).
 - [19] K. Vahala *et al.*, *Nat. Phys.* **5**, 682 (2009).
 - [20] B. Ravindra and A. K. Mallik, *Phys. Rev. E* **49**, 4950 (1994).
 - [21] As the lifetime of the $P_{1/2}$ level (8 ns) is much shorter than the oscillation period (228 ns), the photon-scattering rate adjusts instantaneously as the ion's velocity varies.
 - [22] R. Lifshitz and M. C. Cross, *Rev. Nonlin. Dyn. Complex.* **1**, 1 (2008).
 - [23] S. Zaitsev, O. Shtempluck, E. Buks, and O. Gottlieb, e-print arXiv:0911.0833v2.
 - [24] The ratio between the two terms depends on the laser-cooling detuning and is always below 0.2.
 - [25] M. J. Biercuk, H. Uys, J. W. Britton, A. P. VanDevender, and J. J. Bollinger, *Nature Nanotechnology* **5**, 646 (2010).